Journal of Power Sources 196 (2011) 2779–2784

Contents lists available at ScienceDirect

Journal of Power Sources

journal homepage: www.elsevier.com/locate/jpowsour

The conversion among reactions at Ni-based anodes in solid oxide fuel cells with low concentrations of dry methane

Hongxin You[a,*], Hongjie Gao[a], Gang Chen[b], Abuliti Abudula[b], Xinwei Ding[a]

[a] Institute of Chemical Technology, Dalian University of Technology, Dalian 116012, China
[b] North Japan New Energy Research Center, Hirosaki University, Hirosaki 036-8561, Japan

ARTICLE INFO

Article history:
Received 13 September 2010
Accepted 23 September 2010
Available online 1 October 2010

Keywords:
Solid oxide fuel cell
Anode
Methane
Reaction

ABSTRACT

Dry methane with different concentrations is directly fed to solid oxide fuel cells (SOFCs) with a Ni-yttria-stabilized zirconia (Ni-YSZ) anode and a Ni-scandia-stabilized zirconia (Ni-ScSZ) anode. The anode outlet gases are measured in situ by gas chromatography (GC) to study the reactions of dry methane at different current densities. The comparison between the measured open-circuit voltages (OCVs) and theoretical values, the quantitative analysis of components under different current densities and the activation energy analysis of elementary reactions of CH_4 are investigated to identify the types of reactions occurring to methane in SOFCs. It is found that reactions of partial oxidation, $CH_4 + 2O^{2-} \rightarrow CO + H_2O + H_2 + 4e^-$, $CH_4 + 3O^{2-} \rightarrow CO + 2H_2O + 6e^-$, and complete oxidation occur to CH_4 at the Ni-based anodes in sequence while the current density increasing.

1. Introduction

Solid oxide fuel cells (SOFCs) operating directly on hydrocarbon fuels without external reformation are expected to be an important technology for power generation in the near future.

Carbon deposition during the reaction process is the primary issue for SOFCs with the direct use of hydrocarbon fuels. To overcome this problem, many researchers have been working on anti-coking anode materials. However, research on the anode reaction mechanisms of methane is necessary. Many reactions may take place on the anode side, and various electrochemical reactions will generate different products and heat output. Therefore, appropriate thermal management in the fuel cells is required. In addition, synthesis gases, as the reaction products of methane, are also raw materials for other chemical products. So, it is of great interest to obtain synthesis gases through the control of methane reactions in the process of generating electricity.

It is difficult to identify the electrochemical reactions of methane because of the coexistence of various gases on the anode side. Several authors [1–4] reported that the electrochemical reactions of methane at different current densities are controlled by multifarious factors. At a low current density (low oxygen stoichiometry), the anode reaction mechanism is dominated by methane cracking, while at a higher current density (higher oxygen stoichiometry), it is dominated by the total oxidation of methane. This change in mechanism was confirmed by M.K. Bruce by measuring the cell open-circuit voltage as a function of fuel, CO_2 and H_2O partial pressure and analyzing the SOFC product stream [1]. Kdendall [2] concluded that partial oxidation of methane (POM) occurs in pure methane under an open-circuit by comparing the measured OCV with the theoretical value.

Abudula [3] investigated the methane reactions in a Ni-YSZ anode cell with 4.2% dry methane. By analyzing the amount of electrons quantitatively, it was found that the partial electrochemical oxidation of methane (POM) takes place at a low-current density, while the complete oxidation of methane (COM) occurs at a high current density.

Zhang et al. [4] found that the anode potential dominates the selectivity of products and a low anode polarization assists in generating synthesis gas at a high H_2/CO ratio. However, the current density range studied was from 0 to 100 mA cm^{-2}, which could not reflect the condition of higher current density for methane reactions. Zhan et al. [5] reported that the species and amount of the outlet gases were mainly controlled by the ratio of O^{2-}/CH_4. The contents of H_2 and CO increased to a maximum value as O_2/CH_4 rose to approximately 0.7 and decreased as O_2/CH_4 increased further. The content of CH_4 decreased with increasing O_2/CH_4. The concentration of CO_2 remained low at a low ratio of O_2/CH_4 but increased more rapidly when O_2/CH_4 rose over 0.7. Compared with the anode potential, the ratio of O^{2-}/CH_4 has a greater effect on the methane reactions.

Hecht et al. [6] and Wu and Wang [7] analyzed and calculated the activation energy of each elementary reaction of methane at the Ni-based catalyst. Methane dissociation has two main paths, including direct dissociation and dissociation assisted by oxygen. The activation energy and reaction heat of each elementary reaction

* Corresponding author. Tel.: +86 411 39608115; fax: +86 411 39608115.
E-mail address: youhx@sina.com (H. You).

0378-7753/$ – see front matter © 2010 Elsevier B.V. All rights reserved.
doi:10.1016/j.jpowsour.2010.09.082

for the direct dissociation of methane are significantly smaller than those of methane dissociation assisted by oxygen. Therefore, the direct dissociation is much easier than the dissociation assisted by oxygen for methane. Moreover, the primary path to produce CO is the oxidation reaction of CH(s), and the further oxidation of CO(s) produces CO_2 [7].

Many studies on methane reactions were carried out under fixed operating conditions such as current density or temperature. However, little attention has been paid to the research on the methane reactions in a continuously changing current density range. It is known that the concentration of oxygen ions transported to the anode increases with increasing current. One mole of methane consumes one mole of oxygen ions when POM takes place, while one mole of methane consumes four moles of oxygen ions when COM takes place. However, methane reactions at the anode need to be further studied for the condition of $1 \le \nu(O^{2-})/\nu(CH_4) \le 4$, wherein $\nu(CH_4)$ is the consumption rate of methane involved in the reactions after deducting the part used to produce carbon deposition.

In this paper, the comparison between the measured OCV and theoretical one, the quantitative analysis of elements under different current densities and the activation energy analysis of elementary reactions of CH_4 were investigated to identify the types of reactions occurring to methane at the Ni-based anodes.

2. Experimental

Disks of 8 mol% Y_2O_3–ZrO_2 (8-YSZ; diameter 20 mm; thickness 1 mm, manufactured by Tosoh Company) were used as electrolytes. NiO and YSZ or ScSZ powders in a weight ratio of 3:2 were mixed and ground. 30 wt% (relative to anode composites materials) of pore-forming agents and adhesives consisting of α-terpineol and ethyl cellulose in a weight ratio of 4:1 were added into the mixture and the mixture was kept grounding. Then the anode slurry was prepared onto the electrolyte substrates by the slurry coating method, and the half cells were subsequently sintered at 1400 °C for 2 h in air. The $La_{0.85}Sr_{0.15}MnO_{3-\delta}$ (LSM) cathodes were prepared using a similar method as that did to the anodes on the opposite side of the YSZ disk. The active area of the anodes and cathodes was 0.78 cm^2, and the thickness of them was between 30 μm and 50 μm.

The cell was clamped in the same way as mentioned in Ref. [5]. The furnace was heated to 1000 °C electrically. Pure hydrogen was fed to the anode chamber for 30 min for the reduction of NiO, and then it was purged out with argon. Methane pumped into the anode was diluted into the required concentrations with 50 mL STP min^{-1} argon. The anode gage pressure was 0.1 MPa. The residence time for fuel gas in the anodes, assuming plug flow, was approximately 0.0027–0.0036 s. Pure O_2 was used as an oxidant with an inlet rate of 50 mL STP min^{-1}. The measurements did not start until the OCV became stable. The anode outlet gases were measured in situ with the Agilent GC 7890A gas chromatography system. 15 Min after the current was changed, the GC measurement was conducted.

3. Results and discussion

3.1. Electrical performance

Fig. 1 shows the typical *I–V* curves of the fuel cells with Ni-YSZ and Ni-ScSZ anodes at 1000 °C. Dry methane with different concentrations (3.85% CH_4 + 96.15% Ar and 5.66% CH_4 + 94.34% Ar) were used as fuel. The OCVs of SOFCs with Ni-YSZ and Ni-ScSZ anodes were 1.496 V and 1.495 V, respectively, indicating that both cells were well sealed.

As shown in Fig. 1, the output voltage decreased rapidly in the range of 0.448–0.512 A cm^{-2} for the SOFC based on Ni-YSZ anode.

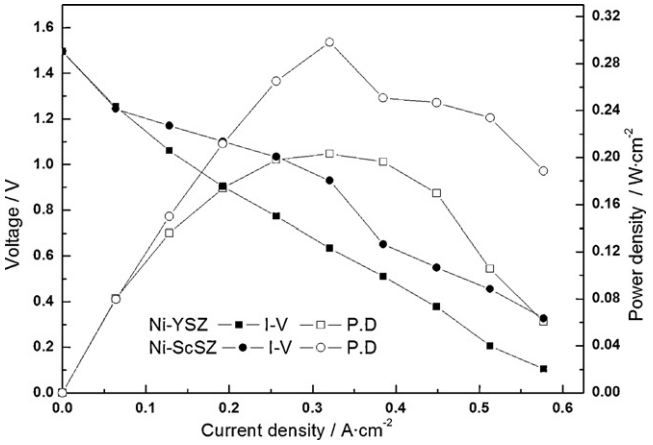

Fig. 1. Curves of *I–V* and power density for fuel cells based on Ni-YSZ and Ni-ScSZ anodes with 3.85% and 5.66% methane, respectively.

The maximum current and power densities were 0.60 A cm^{-2} and 0.29 W cm^{-2}, respectively, for the SOFC based on Ni-ScSZ anode. However, the output voltage as well as the corresponding power density decreased rapidly when the current density was greater than 0.321 A cm^{-2}. Obviously, the electrical performance of the SOFC based on Ni-ScSZ anode is better than that of the cell based on Ni-YSZ anode. The result is due to the higher electrical conductivity of ScSZ. The conductivity of the scandia-doped system (ScSZ) is around 0.3 S cm^{-1} at 1000 °C, which is three times higher than that of 8YSZ [8].

3.2. Analysis of outlet gases

Figs. 2 and 3 show the production rates of anode outlet gases for SOFC with 3.85% and 5.66% methane, respectively.

The carbon deposition rate is calculated by the carbon balance equation:

$$\nu(C)_{dep} = \nu(CH_4)_{in} - \nu(CH_4)_{out} - \nu(CO)_{out} - \nu(CO_2)_{out} \quad (1)$$

where $\nu(C)_{dep}$ is the flux of deposited carbon per second, $\nu(CH_4)_{in}$ is the inlet flux of CH_4, $\nu(CH_4)_{out}$, $\nu(CO)_{out}$ and $\nu(CO_2)_{out}$ are the outlet fluxes of CH_4, CO and CO_2, respectively.

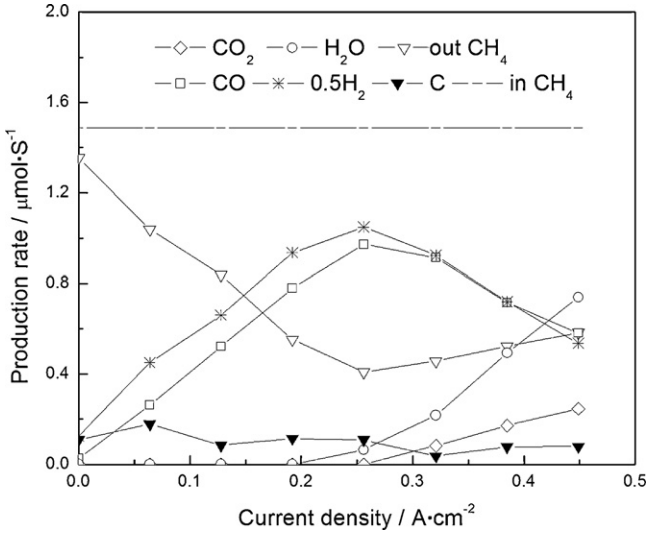

Fig. 2. Production rates of anode exhaust gases in SOFC with Ni-YSZ anode and 3.85% methane.

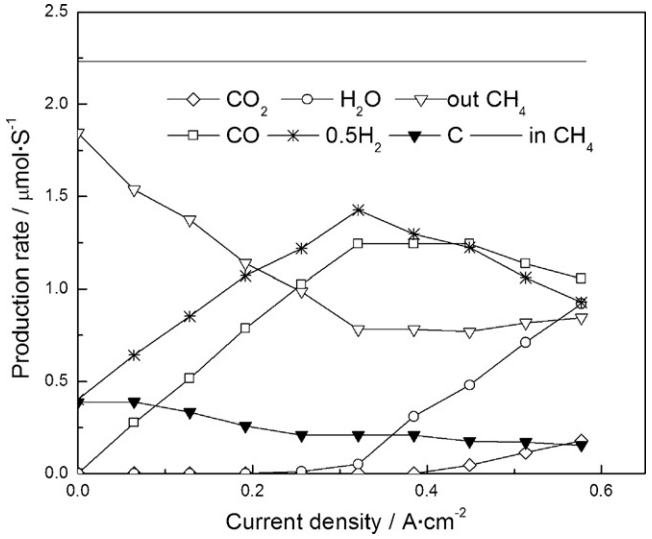

Fig. 3. Production rates of anode exhaust gases in SOFC with Ni-ScSZ anode and 5.66% methane.

The flux of water is calculated from the hydrogen balance by the following equation:

$$\nu(H_2O)_{fH} = 2[\nu(CH_4)_{in} - \nu(CH_4)_{out}] - \nu(H_2)_{out} \quad (2)$$

The water generation rate can also be calculated by using the oxygen balance equation:

$$\nu(H_2O)_{fO} = \nu(O^{2-}) - \nu(CO)_{out} - 2\nu(CO_2)_{out} \quad (3)$$

where $\nu(O^{2-})$ is the O^{2-} flux calculated from the current (I) passing through the electrolyte. The relation between the $\nu(O^{2-})$ and I is

$$\nu(O^{2-}) = \frac{I}{2F} \quad (4)$$

where F is the Faraday constant. Here $\nu(H_2O)$ was calculated from the oxygen according to (3) due to the accurate current. Both curves of H_2 in Figs. 2 and 3 were drawn with one-half calculated production rate.

Different concentrations of methane produce different production rates of outlet gases. As shown in Figs. 2 and 3, the production rates of CO and H_2 increased linearly with current density at first and then decreased after reaching the maximum. Furthermore, neither CO_2 nor H_2O was generated under low current density. However, they began to emerge when the amount of desorption of CO and H_2 decreased. And H_2O was observed earlier than CO_2 in the outlet gases.

The amount of outlet methane decreased rapidly as the current density increased, indicating that more methane was consumed. After the production rates of CO and H_2 reached the peak values, the production rate of H_2 decreased with a higher speed than that of CO. The production rate of CO maintained at a steady high level in a small range and then decreased gradually, as seen in Fig. 3. Subsequently, the outlet flux of methane had no significant change and decreased gradually to a lower level.

3.3. Analysis of the anode reaction

Methane can decompose anywhere including at the three-phase boundary (TPB) on the anode side at high temperature. The decomposition products are able to react with the oxygen ions from the cathode side. Moreover, the methane can also be adsorbed on the anode catalyst and react with the oxygen ions directly [4].

The outlet gases in the anode chamber contained CO, H_2, CO_2, H_2O and some residual CH_4. Including the deposited carbon, there were six components on the anode side. Certain species may cause electrochemical reactions with the O^{2-} from the cathode side. Chemical reactions can take place among six species. The possible electrochemical reactions are listed as below:

$$CH_4 + 4O^{2-} \rightarrow CO_2 + 2H_2O + 8e^- [8–10] \quad (5)$$

$$CH_4 + O^{2-} \rightarrow CO + 2H_2 + 2e^- [8–10] \quad (6)$$

$$CH_4 + 2O^{2-} \rightarrow CO + H_2 + H_2O + 4e^- [4, 10] \quad (7)$$

$$CH_4 + 2O^{2-} \rightarrow CO_2 + 2H_2 + 4e^- [11] \quad (8)$$

$$CH_4 + 3O^{2-} \rightarrow CO + 2H_2O + 6e^- [12, 13] \quad (9)$$

$$CH_4 + 3O^{2-} \rightarrow CO_2 + H_2 + H_2O + 6e^- \quad (10)$$

$$H_2 + O^{2-} \rightarrow H_2O + 2e^- [9, 10] \quad (11)$$

$$CO + O^{2-} \rightarrow CO_2 + 2e^- [10, 11] \quad (12)$$

$$C + O^{2-} \rightarrow CO + 2e^- [10, 11] \quad (13)$$

The possible chemical reactions are listed as below:

$$CH_4 \rightarrow C + 2H_2 [8–11, 14, 15] \quad (14)$$

$$CH_4 + H_2O \rightarrow CO + 3H_2 [3, 10] \quad (15)$$

$$CO + H_2O \rightarrow CO_2 + H_2 [9, 10, 11] \quad (16)$$

$$CH_4 + CO_2 \rightarrow 2CO + 2H_2 [9, 10] \quad (17)$$

$$2CO \rightarrow C + CO_2 [9, 10, 15] \quad (18)$$

$$C + H_2O \rightarrow CO + H_2 [3, 15] \quad (19)$$

Among the above reactions, some are not independent. For example, POM can be regarded as the integration of reactions of high-temperature decomposition of CH_4 and carbon oxidation. It can also be interpreted that the high-temperature decomposition of methane occurs first, and then the carbon reacts with O^{2-} to form CO. The reaction (5) is COM which demands that sufficient amount of oxygen ions are transported from the cathode. Similarly, COM can be regarded as the integration of reactions of high-temperature decomposition of CH_4, carbon oxidation, hydrogen oxidation and CO oxidation. Reaction (9) can also be regarded as the integration of reactions of high-temperature decomposition of CH_4, carbon oxidation and hydrogen oxidation. Therefore, each oxidation reaction of methane at the anode can be seen as combinations of the following basic reactions in the macroscopic view: decomposition of methane, hydrogen oxidation, C oxidation, and CO oxidation, independent of the type of micro-mechanism it undergoes.

Through the analysis above, it can be found that the production rates of the outlet gases of both cells based on Ni-YSZ anode and Ni-ScSZ anode have similar change tendencies. In this paper, the cell based on Ni-YSZ anode was mainly investigated for the research on methane reactions at Ni-based anodes.

3.3.1. Analysis of open circuit voltage

In this study, the OCV of the Ni-YSZ anode cell with 3.85% methane was 1.496 V. The standard electromotive forces of COM, reaction (7), POM and hydrogen oxidation calculated by the Nernst equation were 1.090 V, 1.204 V, 1.444 V and 0.923 V, respectively [4]. Among these values, the standard electromotive force of POM is the closest to the measured OCV. However, the measured OCV is slightly higher than the standard electromotive force of POM. The

Nernst equation for POM is shown below:

$$\begin{aligned} E &= E^{\theta} - \frac{RT}{ZF}\ln\left[\frac{(P_{CO}/P_0)(P_{H_2}/P_0)^2}{(P_{CH_4}/P_0)(P_{O_2}/P_0)^{1/2}}\right] \\ &= 1.444 - 0.0548\ln\left[\frac{(P_{CO}/P_0)(P_{H_2}/P_0)^2}{(P_{CH_4}/P_0)(P_{O_2}/P_0)^{1/2}}\right] \\ &= 1.444 - 0.0548\ln\left[\frac{(x_{CO}P_{anode}/P_0)(x_{H_2}P_{anode}/P_0)^2}{(x_{CH_4}P_{anode}/P_0)(P_{O_2}/P_0)^{1/2}}\right] \\ &= 1.444 - 0.0548\ln\left[\frac{4x_{CO}^3(P_{anode}/P_0)^2}{x_{CH_4}(P_{O_2}/P_0)^{1/2}}\right] \end{aligned} \quad (20)$$

where P_{anode} is the absolute pressure of the anode chamber, P_0 is the standard atmospheric pressure, and x_{CO}, x_{H_2} and x_{CH_4} are the mole fraction of CO, H_2 and CH_4, respectively. In theory, there is no CO in the anode chamber under open-circuit. However, a small amount of CO is present at the moment. The presence of CO might be due to the residual oxygen or by the O^{2-} transported from the cathode because of the small current existing in cells. In this study, $P_{anode}/P_0 = 2$. The OCV of the SOFC based on Ni-YSZ anode can achieve 1.496 V at 1000 °C when $(P_{O_2}/P_0)^{1/2} = 4.59 \times 10^{-7}$, which is higher than the standard cell potential of 1.444 V. This indicates that POM occurred at the Ni-YSZ anode under open-circuit.

3.3.2. Analysis of outlet gases

The measured outlet gases only contained CO, H_2 and residue methane when the current density was lower than 0.192 A cm^{-2}. Therefore, the reactions of hydrogen oxidation and CO oxidation were excluded and the steam reforming reaction (15), shift reaction (16), CO_2 reforming reaction (17) and C gasification reaction (19) were also ruled out. The reason for the shift reaction and CO_2 reforming reaction were ruled out is that no CO_2 was detected out by GC at low current density. However, there is a possibility that the CO_2 formed by the CO oxidation reaction had been consumed by the CO_2 reforming reaction (17). According to the relationship between the products and reactants, if the CO_2 reforming reaction occurs, the amount of CO generated from reaction (17) should be twice as much as that of consumed CH_4, and the ratio of the H_2 production rate to CO production rate should be one. In fact, from the GC analysis results, it can be seen that the ratio between H_2 and CO production rates is greater than 2 and the ratio of the amount of CH_4 consumed to the amount of CO generated is almost 1. Therefore, reaction (17) does not happen at this moment. At low current density, we can conclude that the steam reforming reaction of methane (15) does not occur because if it takes place, the amount of H_2 formed should be three times as much as that of CO generated, which contradicts with the measurement results. In addition, H_2O is needed in the steam reforming reaction. However, water-free dry methane was used in this experiment. Therefore, the steam reforming reaction could be carried out only after water is generated from hydrogen oxidation. The GC analysis shows that the amount of hydrogen is twice as much as that of CO in the outlet gases. It can be seen from Fig. 2 that the production rate of CO is proportional to the current density, and no CO_2 existed in the range of 0–0.192 A cm^{-2}, which proves that the shift reaction (16) also does not happen at low current density. Similarly, no C gasification reaction (19) occurs due to the use of water-free dry methane.

The above analysis shows that no pure chemical reactions took place except the high-temperature decomposition reaction of methane in the range of 0–0.192 A cm^{-2}. Therefore, the H_2 and CO were solely generated from the electrochemical partial oxidation reaction of methane.

In the current density range of 0.192–0.256 A cm^{-2}, there was an obvious reaction which can generate H_2O along with the POM. The only electrochemical oxidation reaction of methane which can simultaneously generate CO, H_2 and H_2O is reaction (7). It can produce CO, H_2 and H_2O while generating power. The standard potential of this reaction is 1.204 V. Moreover, its molar enthalpy change and Gibbs free energy change are $\Delta H^{1273} = -246.871$ kJ mol^{-1} and $\Delta G^{1273} = -464.731$ kJ mol^{-1}, respectively at 1273 K [4]. The negative ΔG of reaction (7) indicates that the reaction can take place independently once the reaction conditions are met.

There was more H_2O formed on the anode TPB with increasing current density, from which it can be deduced that the reaction (9) took place. Correspondingly, the production rate of H_2O increases faster as shown in Fig. 2.

In the process of the current density increasing from 0.192 A cm^{-2} to 0.256 A cm^{-2}, more CO was generated through the electrochemical oxidation reaction of methane on the anode TPB. Once the current density exceeded 0.256 A cm^{-2}, CO_2 began to appear in the anode outlet gases. There are many ways to generate CO_2, including the direct oxidation of the deposited carbon, the oxidation of CO, COM, shift reaction of CO and the disproportion reaction of CO. The GC measurements showed that CO was formed firstly. If CO_2 was formed by the direct oxidation of carbon, there should be CO_2 in the outlet gases. Furthermore, it is difficult for CO to be used as fuel directly in fuel cells under the conditions of H_2 and CO co-existence [16], because there is a greater polarization for the oxidation reaction of CO, especially in the case of existence of water vapor. If CO_2 is generated through the steam reforming-shift reaction of methane:

$$CH_4 + 2H_2O \rightarrow CO_2 + 4H_2 \quad (21)$$

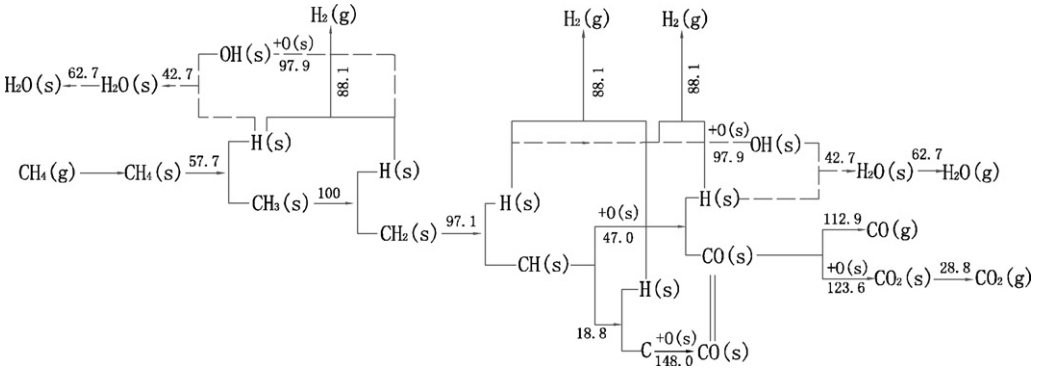

Fig. 4. Reaction steps of methane at Ni-YSZ anode.

the production rate of H_2 will increase sharply along with increasing current density. In fact, the hydrogen in the outlet gases decreased gradually when the current density increased to 0.256 A cm^{-2}.

CO_2 may be produced through reactions (8), (10) and (5). Therefore, reactions of methane may occur at the Ni-YSZ anode through three paths in the entire process, namely Path 1 (reactions (6), (7), (9) and (8)), Path 2 (reactions (6), (7), (9) and (10)) and Path 3 (reactions (6), (7), (9) and (5)).

3.3.3. Activation energy analysis

Refs. [6,7] provide the activation energy of each elementary reaction of methane reacting with O^{2-} at the Ni-YSZ anode. The reaction steps of methane at the Ni-YSZ anode are summarized in Fig. 4. It is based on the principle that elementary reactions with smaller activation energies occur more readily. The unit of the activation energy E_a is kJ mol^{-1}.

Before the electrochemical oxidation reactions of methane occurred, the methane was first dissociated directly into H(s) and CH(s). Subsequently, H_2 was generated from the combination and desorption of H(s), and CH(s) was continuously dissociated to generate C at the same time.

The possibility for each elementary reaction of methane oxidation depends on the activation energy of the methane decomposition species reacting with O^{2-}. When O^{2-} emerged at the anode TPB, the species from the direct dissociation of methane could react with O^{2-}. Among them, some CH(s) reacted with O^{2-} into CO(s), in which its activation energy is the lowest, 47.0 kJ mol^{-1}. And the activation energy of CO(s) desorption is less than that of CO(s) reacting with O^{2-} into CO_2(s). Therefore, CO emerged first. H_2O was not generated at this moment because the aggregation and desorption of H(s) took place preceding H(s) + O(s) → OH(s). As a result, CO and H_2 were generated at the same time in this process, which indicated that the POM occurred. It can be seen from Fig. 2 that the outlet gases only contained CO and H_2 in the range of 0–0.192 A cm^{-2}. However, the amount of CH(s) reacting with O^{2-} into CO(s) was less than that formed from the direct dissociation of methane. Therefore, the high-temperature decomposition reaction and partial oxidation of methane took place simultaneously in the low current density range.

The amount of O^{2-} on the anode TPB increased with the current density under constant temperature. The probability of O^{2-} involving in reactions increased. The O^{2-} would either participate in H(s) + O(s) → OH(s), E_a = 97.9 kJ mol^{-1} in which OH(s) would react with H(s) to form H_2O, or it would participate in CO(s) + O(s) → CO_2(s), E_a = 123.6 kJ mol^{-1} and then CO_2 was formed after desorption. However, a large amount of H(s) was accumulated on the anode TPB, and the activation energy of H(s) + O(s) → OH(s) is less than that of CO(s) + O(s) → CO_2(s), so H_2O should be generated before CO_2 at the anode. As a result, reactions (8) and (10) did not take place until H_2O was generated. It is evident that the reaction of CH_4 would not take place at the anode through Paths 1 and 2.

At the beginning of H_2O generation, only a part of H(s) was converted into H_2O because there was no sufficient O^{2-} to react with H(s). Then rich H(s) continued to combine and generate H_2 after desorption. The direct dissociation reactions of methane and the elementary reactions which generated CO, H_2 and H_2O were fitted together to obtain the reaction (7). When the amount of O^{2-} was sufficient to oxidize H(s) into H_2O completely, reaction (7) was converted to reaction (9). When reaction (7) and (9) occurred in sequence, the production rate of H_2 in the outlet gases decreased faster and faster. Meanwhile, H_2 was still presented as a result of the ongoing partial oxidation.

The standard electromotive force is 1.204 V for the reaction of $CH_4 + 2O^{2-} \rightarrow CO + H_2 + H_2O + 4e^-$ occurred in the Ni-ScSZ anode cell at 1000 °C. This value is 0.240 V lower than 1.444 V of the POM. When the dominant reaction of dry methane at the Ni-ScSZ anode transitioned suddenly from the POM to the reaction of $CH_4 + 2O^{2-} \rightarrow CO + H_2 + H_2O + 4e^-$, it would cause the OCV dropping down. For the consideration of various polarization losses, the output voltage of the cell would also decrease further. Therefore, when the current density of the Ni-ScSZ anode cell exceeded 0.321 A cm^{-2}, its output voltage decreased rapidly. Similarly, the same trend existed in the Ni-YSZ anode cell when its current density was in the range of 0.448–0.512 A cm^{-2}.

O^{2-} is involved in the higher activation energy reactions as its amount increases with increasing current. The CO_2 then began to emerge in the anode chamber because the activation energy of CO(s) + O(s) → CO_2(s), E_a = 123.6 kJ mol^{-1} is less than that of C(s) + O(s) → CO(s), E_a = 148.0 kJ mol^{-1}. Reaction (9) occurred before CO_2 was generated. After CO_2 formed, reaction (5) took place along with reaction (9).

According to the above analysis, it can be concluded that methane reacts with O^{2-} at the Ni-YSZ anode through Path 3 (reactions (6), (7), (9) and (5) take place in sequence) and the high-temperature decomposition of methane takes place throughout the entire process.

According to the same analysis, we can also obtain the conclusion that the electrochemical oxidation reactions of methane take place following Path 3 in the Ni-ScSZ cell with 5.66% dry methane with the continuously increasing current density.

4. Conclusions

Low concentrations of dry methane were fed to the anode chambers of Ni-YSZ/YSZ/LSM and Ni-ScSZ/YSZ/LSM fuel cells. The electrochemical reactions of methane at the anodes were studied under a varying current density. The comparison between the open-circuit voltages (OCV) and theoretical OCV, the quantitative analysis of elements at different current densities as well as the analysis of the activation energy of elementary reactions of CH_4 were investigated to identify the types of methane reactions. It was found that electrochemical oxidation reactions of methane take place according to the following sequence with increasing current density:

$$CH_4 + O^{2-} \rightarrow CO + 2H_2 + 2e^-$$

$$CH_4 + 2O^{2-} \rightarrow CO + H_2O + H_2 + 4e^-$$

$$CH_4 + 3O^{2-} \rightarrow CO + 2H_2O + 6e^-$$

$$CH_4 + 4O^{2-} \rightarrow CO_2 + 2H_2O + 8e^-$$

When the latter reactions that consume much more O^{2-} take place, the former reactions that consume relatively less O^{2-} are still ongoing. However, since the rates of the former reactions slow down, the corresponding output rates of the products will also decrease.

References

[1] M.K. Bruce, M.V.D. Bossche, S. McIntosh, J. Electrochem. Soc. 155 (2008) B1202–B1209.
[2] K. Kdendall, C.M. Finnerty, G. Sauunders, et al., J. Power Sources 106 (2002) 323–327.
[3] A. Abudula, M. Ihara, H. Komiyama, et al., Solid State Ionics 86–88 (1996) 1203–1209.
[4] X. Zhang, S. Ohara, H. Chen, et al., Fuel 81 (2002) 989–996.
[5] Z.L. Zhan, Y.B. Lin, M. Pillai, et al., J. Power Sources 161 (2006) 460–465.
[6] E.S. Hecht, G.K. Gupta, H.Y. Zhu, Appl. Catal. A 295 (2005) 40–51.
[7] T.H. Wu, H.Y. Wang, J. Zhejiang Normal Univ. (Nat. Sci.) 19 (1996) 48–52.
[8] O. Yamamoto, Y. Arati, Y. Takeda, Solid State Ionics 79 (1995) 137–142.
[9] H.X. You, A. Abudula, X.W. Ding, et al., J. Power Sources 165 (2007) 722–727.

[10] J.-H. Koh, Y.-S. Yoo, J.-W. Park, et al., Solid State Ionics 149 (2) (2002) 157–166.
[11] K. Ke, A. Gunji, H. Mori, S. Tsuchida, et al., Solid State Ionics 177 (2006) 541–547.
[12] A. Sin, E. Kopnin, Y. Dubitsky, A. Zaopo, et al., J. Power Sources 145 (2005) 68–73.
[13] Y. Nabae, I. Yamanaka, Appl. Catal. A 369 (2009) 119–124.
[14] H. Sumi, K. Ukai, Y. Mizutani, et al., Solid State Ionics 174 (2004) 151–156.
[15] A. Gunji, C. Wen, J. Otomo, et al., J. Power Sources 131 (2004) 285–288.
[16] A.M. Sukeshini, B. Habibzadeh, B.P. Becker, et al., J. Electrochem. Soc. 153 (2006) A705–A715.